Heat-dependent gird melting drives TRPV1 opening

Running title: Digit codes for heat-gated TRPV1

Guangyu Wang*

Department of Physiology and Membrane Biology, University of California School of Medicine, Davis, CA, USA

Department of Drug Research and Development, Institute of Biophysical Medico-chemistry, Reno, NV, USA

* Correspondence: E-mail: gary.wang10@gmail.com

Abstract

Non-covalent interactions in bio-macromolecules are individually weak but collectively important. How they take a concerted action in a complex biochemical reaction network to realize their thermal activity and stability is still challenging to study. Here graph theory was used to investigate how the temperature-dependent non-covalent interactions as identified in the structures of the thermo-gated capsaicin receptor TRPV1 could form a grid-like mesh network with topological grids to maintain the 3D structure of TRPV1 and to govern heat-sensing. The results showed that the heat-evoked melting of the biggest grid may initiate a specific temperature threshold for both channel activation and inactivation while a thermostable balance between an open state and a putative inactivated state from a pre-open closed state may account for heat efficacy and the use-dependent desensitization. Altogether, both the biggest and smaller grids may be necessary for the lipid-dependent temperature sensitivity. Therefore, this grid thermodynamic model may be broadly significant for thermal stability and activity of biological macromolecules.

Keywords: desensitization, grid thermodynamics, lipid, non-covalent interaction, systemic thermal instability, temperature sensitivity, threshold, TRP channel

1. INTRODUCTION

Temperature is important in everyday life. Transient receptor potential (TRP) vanilloid-1 (TRPV1) is well-known as a noxious heat sensor in a primary afferent neuron of the dorsal root and the trigeminal ganglia. Its activation allows sodium or calcium to be permeable to a channel pore. With an activation threshold (~42 °C) above a normal human body temperature 37 °C and a temperature coefficient Q_{10} (the ratio of rates or open probabilities (P_o) of an ion channel measured 10 °C apart) higher than 20, this channel can work as a bio-thermometer to monitor a noxious heat signal above 42 °C and to regulate the human body temperature. [1-4] In addition to the physical stimuli, capsaicin can also activate TRPV1, producing hot sensation. As cold can decrease the capsaicin-evoked activity of TRPV1, [5] the same gating pathway seems to be shared by both stimuli. On the other hand, residues sensitive to both physical and chemical stimuli are different in TRPV1, suggesting their distinct gating pathways. [6-9]

TRPV1 is a homotetramer with each monomer consisting of six transmembrane helices. The first four segments (S1–S4) form a voltage-sensor-like domain (VSLD) while the last two (S5 and S6), together with the intervening loop and the pore helix and the extracellular cap-like pore turret between S5 and S6, are folded as a pore domain. The pore domain is surrounded by the VSLD in a domain-swapped arrangement. The cation conductance pathway centers in the pore domain. A hydrophobic constriction around I697 forms a lower S6 gate while the segment from G643 to D646 (^{643}GMGD^{646}) between S5 and S6 (S5-P-S6) in rat TRPV1 (rTRPV1) acts as a short selectivity filter. The S4–S5 linker, which is a short amphipathic helix and almost parallel to the cytoplasmic membrane, couples the VSLD with the pore domain for channel gating. Thus, the overall structure of the TRPV1 channel resembles that of the voltage-gated ion channel. [10-11] However, TRPV1 has a conserved TRP domain, which runs parallel to the inner leaflet of the membrane by virtue of a sharp bend after S6, not only linking the S6 gate crossing bundle but also interacting with the S4–S5 linker and the pre-S1 domain in favor of allosteric coupling between different gating domains. In addition, the characteristic ankyrin repeats within the cytoplasmic N terminus can tether cytoplasmic N- and C-terminal domains for channel assembly. [11-14] Although the structural basis for the chemical stimuli such as capsaicin has been clear, [6, 15-16] the heat-evoked gating pathway is still unknown for TRPV1. The remaining questions include what structural factors or motifs control the specific temperature threshold 42 °C, [17] how the phosphatidylinositol (PI) lipid at the capsaicin site increases the temperature sensitivity Q_{10} from

16.4 to 28.2, [14] and what structural factors or motifs govern the use-dependent desensitization above 42 °C in an irreversible manner. [1, 8, 18-19]

Since 2013 a DNA hairpin thermal sensor with a limited poly-A loop length has been created to monitor a change in a biological microenvironment. When temperature increases above a threshold in a range from 34 °C to 73 °C, the hydrogen bonds between the bases in the DNA duplex are broken so that the DNA hairpin melts with a characteristic sigmoid plot. [20] Similarly, TRPV1 can be activated above a specific temperature threshold 42 °C and also with a featured sigmoid plot at elevated temperatures. [17] Because a grid in a grid-like non-covalent interaction mesh network is topologically similar to a DNA hairpin in general term and removing this network grid by heat is analogous to DNA hairpin melting, it is fitting to ask if the thermosensitive TRPV1 channel exploits a series of temperature-dependent grid-like non-covalently interacting mesh networks to keep the 3D structure of TRPV1 and thus to control heat-sensing.

In this computational study, graph theory was used as a novel tool to evaluate the role of each grid in the individual grid-like non-covalently interacting mesh networks as found in the cryo-electron microscopy (cryo-EM) structural data of rTRPV1 with or without PI-bound at the capsaicin site around the temperature thresholds [14]. Since the temperature threshold above 34 °C can be raised more than 20 degrees when the loop length in a DNA hairpin declines from 20 to 10 A's or the H-bonded G-C base-pairs double from 2 to 4, the size and the strength of a grid may play a critical role in the melting temperaure. After the grid size (S) was defined by graph theory as the minimal number of the total side chains of residues in protein or atoms in the bound lipid that did not participate in any non-covalent interctions in a grid, the biggest grid along the gating pathway could then be identified. When the number of grid size-controlled non-covalent interactions equivalent to H-bonds were available in the biggest grid, the melting temperature (T_m) could be calculated approximately. [20] If the biggest grid undergoes the single-rate-limiting-step melting reaction in TRPV1 gating like DNA hairpins, the calculated T_m should be comparable to the experimental thresholds (T_{th}).

When the biggest grid melts above a temperature threshold, the whole grid-like non-covalent interaction mesh network will inevitably rearrange along the gating pathway. Accordingly, it is necessary to evaluate the grid-based systemic thermal instability (T_i) of different gating states with a reasonable energetic sequence to develop an integrative physiological model which can link crystallographic static conformations with electrophysiological dynamic findings

together very well for the use-dependent heat desensitization of TRPV1. As a DNA hairpin is more thermostable with smaller loops or more H-bonds in the stem, T_i of a given gating state in TRPV1 was hence defined as a ratio of the total grid sizes to the total non-covalent interactions along the same gating pathway.

On the other hand, it has been reported that the opening rate or the open probability (P_o) of TRPV1 is increased at raised temperatures [18, 21]. Thus, if the temperature threshold for TRPV1 opening is determined by a rate-limiting single step to disrupt a non-covalent interaction in the biggest grid along the gating pathway, TRPV1 opening would be enthalpy-driven ($\Delta H<0$) because the dissociation rate (k_d) of enthalpy-driven non-covalent interaction in a biophysical network is factually accelerated at elevated temperatures but k_d of entropy-driven crosslinks is negligibly affected or even slowed under these conditions. [22] In this case, when a thermo-gated TRPV1 opens from a closed state within 10 °C, the functional thermo-sensitivity or the temperature coefficient (Q_{10}) should be governed by the enthalpy-driven changes of the whole grids in the non-covalently interacting mesh networks. In this regard, once the structural thermo-sensitivity (Ω_{10}) was similarly and approximately defined as a heat-evoked change of the total chemical potential of all the grids upon a change in the total enthalpy included in non-covalent interactions along the same gating pathway of one subunit between open and closed or inactivated states within 10 °C apart, Ω_{10} should be comparable to Q_{10}.

Taken together, these three lines of computational and comparative results favored three proposals. First, the melting temperature (T_m) of the biggest grid may be responsible for the specific temperature threshold (T_{th}) for TRPV1 activation and inactivation; Second, a thermostable balance between an open state and a putative inactivated state from a pre-open closed state may determine the heat efficacy and the use-dependent desensitization with a reasonable energetic sequence; Third, the functional thermostability or the temperature coefficient Q_{10} of TRPV1 may be controlled by the grid-based structural thermo-stability Ω_{10} in a PI lipid-dependent manner.

2. RESULTS

2.1. Closed PI-free rTRPV1 at 25 °C had the Biggest $Grid_{21}$ with the calculated T_m 32 °C in the VSLD/Pre-S1 interface

The previous chimera studies between rTRPV1 and rTRPV2 demonstrated that the transmembrane segment 434-687 and the pre-S1 segment 401-415 may be involved in the regulation of the temperature threshold while the pre-S1 segment 358-434 plays a critical role in

mediating the temperature sensitivity Q_{10}. In contrast, an exchange of the C-terminal segment 688-838 has no effect. [17] On the other hand, the prior chimera investigations between heat-sensing TRPV1 and cold-sensing TRP melastatin 8 (TRPM8) indicated that the C-terminal including the TRP domain (693-710) is required for the polarity of thermal sensitivity. [23] Therefore, the segment from D388 in the pre-S1 domain to K710 in the TRP domain should be at least included as the gating pathway for the temperature threshold and sensitivity and the systemic thermal instability. At 25 °C, several kinds of non-covalent interactions between amino acid side chains along this gating pathway of PI-free rTRPV1 formed a biophysical network of topological grids in the closed state (**Fig.1A**).

First, H-bonds between different hydrophilic amino acid side chains contributed to the formation of grids. In the pre-S1/VSLD interface, Q423-D427 and D424-R428 were paired for H-bonding. In the VSLD, T449-W549, R455-Y537-K535-Y463 and Q519-N551 were H-bonded in between. In the VSLD/S4-S5 linker/TRP/VSLD interfaces, the H-bonding pairs were R491-E709, R557-T704 and Q560-K694. In the pore domain and its interface with the TRP domain, pairs D576-T685, Y584-T641 and Q691-N695 were also engaged in H-bonds (**Fig. 1A**).

Second, aromatic π interactions also brought about grids. Most of them were located in the VSLD and its interfaces with the pre-S1 domain. For example, Y401-R499, R499-Y495, F434-W426/F438/Y555, F438-Y555, Y441-F488/F516/Y555, Y444-F448/F488, M445-W549, Y453-Y454, P456-Y463, V486-F490, Y487-F488/R491, F488-F516, F489-I493/L524, Y495/F517-F496, Y511-L515, F516-N551/Y554, F517-L521, F522-F543, Y530-F531/Y537 and Y554-Y555. In the S4-S5 linker/TRP interface, Q560 formed a CH-π interaction with W697. In the pre-S1/TRP interface, R701 produced a cation-π interaction with W426. In the pore domain, the π-interacting pairs had F580-L678, F589-T593, F591/T670-Y666, Y627/E636-F649, F640-Y666, and F649/Y653-F659 (**Fig. 1A**).

Third, salt-bridging pairs included K425-E709 in the pre-S1/TRP interface, R491-E513 and R534-E536 in the VSLD, E648-K656 in the outer pore, and K688-E692 in the S6/TRP interface (**Fig. 1A**).

Taken together, along the gating pathway from D388 to K710, sixty non-covalent interactions produced the total grid sizes as 83 (**Fig. 1A**). Thus, the systemic thermal instability (T_i) of this closed PI-free-rTRPV1 was 1.38 (**Table 1**). Among the multiple grids, despite several smaller ones with 0- to 9- residues sizes, the biggest one was outstanding in the pre-S1/VSLD

interface. It had a 21-residue size via the shortest path from Y401 to Q423, D427, W426, F434, Y555, Y441, F516, F517, F496, R499, and back to Y401 to control the R499-Y401 π interaction (**Figs. 1B-D**). Because two equivalent H-bonds sealed this biggest $Grid_{21}$, the predicted melting temperature was about 32 °C (**Table 1**).

Table 1 New parameters of the rTRPV1 bio-thermometer based on the grid thermodynamic model

Construct	**Control**	**rTRPV1**			
Lipid environment	MSP2N2	MSP2N2			native
PDB ID	7LPE	7LPB	7LPD	7LPC	7LPC
Lipid PI at the capsaicin site	free	free	free	bound	bound
Sampling temperature, °C	**48**	**25**	**48**	**48**	
Gating state	open	closed	Putatively inactivated	closed	closed
Name of the biggest grid	$Grid_9$	$Grid_{21}$	$Grid_{9'}$	$Grid_8$	$Grid_{13}$
Biggest grid size (S_{max})	9	21	9’	8	13
Equivalent H-bonds in S_{max}	2.0	2.0	2.0	2.0	1.5
Total non-covalent interactions	46	60	60	67	65
Total grid sizes, a.a./atoms	66	83	59	86	88
Systemic thermal instability (T_i)	1.43	1.38	0.98	1.28	1.35
Calculated T_m, °C	56	**32**	56	**58**	**43**
Measured threshold T_{th}, °C	**56**	**<48**	56	**>48**	**42**
Calculated $\Omega_{10,\,min}$ at E=0.5 kJ/mol		6.56	-2.07	10.5	10.9
Calculated $\Omega_{10,\,mean}$ at E=1.0 kJ/mol		**16.2**	**-5.10**	**28.8**	**28.7**
Calculated $\Omega_{10,\,max}$ at E=3.0 kJ/mol		70.0	-21.3	143	134
Measured Q_{10}		**16.4**	**-5.09**		**28.2**
References for T_{th} and Q_{10}	[14, 18]	[14]	[18]	[14]	[14, 18]

2.2. PI-free rTRPV1 Opened at 48 °C with the Melting of the Biggest $Grid_{21}$ in the VSLD/pre-S1 Interface

If the biggest $Grid_{21}$ with a 21-residue size in rTRPV1 carries out the single-step melting reaction like DNA hairpins, the calculated melting temperature 32 °C should be enough to open it

above 32 °C (**Table 1**). In agreement with this assumption, when PI-free rTRPV1 opened at 48 °C, the broken R499-Y401 π interaction resulted in the melting of the biggest $Grid_{21}$ in the VSLD/pre-S1 interface together with several changes along the gating pathway.

In the pre-S1/VSLD/TRP interfaces, the K425-E709 salt bridge and the Q423-D427 and D424-R428 and R491-D707 H-bonds were disconnected. In the VSLD/S4-S5 linker/TRP interfaces, when the Y554-Y555 π interaction was disrupted, the H-bond moved from R557-T704 to Y554-T704 and the π interaction shifted from Y555-F438 to F559-F438. When the Q560-K694 H-bond was disrupted, the R557-E570 H-bond and the W697-R701 CH-π interaction were formed (**Fig. 2A**).

When this conformational change extended to the VSLD, the R491-E513 and R534-E536 salt bridges, the R455-Y537-K535-Y463 and Q519-N551 H-bonds, and the Y441/F516-F488 and F489-I493 and Y530-F531 π interactions were disconnected. Meanwhile, the new Y495-R499/S510 H-bonds and the new R499-D509 salt bridge and the new F489-F490 π interaction emerged (**Fig. 2A**).

When this conformational change extended to the pore domain and its interfaces with the S4-S5 linker and the TRP domain, the E648-K656 and K688-E692 salt bridges and the Q691-N695 H-bond were disrupted. In the meanwhile, the new Y584-Y666 and T650-N652 and Y653-K656 H-bonds and the new E651-K656 salt bridge were born (**Fig. 2A**).

By all accounts, the total non-covalent interactions and grid sizes along the gating pathway from D388 to K710 dramatically decreased from 60 and 83 to 46 and 66, respectively (**Fig. 2A**). As a result, the systemic thermal instability (T_i) of the gating pathway was increased from 1.38 to 1.43 along with the mean structural thermo-sensitivity Ω_{10} (16.2), which was close to the experimental Q_{10} (16.4) (**Table 1**). [14] On the other hand, when two equivalent H-bonds sealed the biggest $Grid_9$ with a 9-residue size in the VSLD/S4-S5 linker/TRP interfaces to control the stimulatory R557-E570 H-bond, the melting temperature was about 56 °C (**Fig. 2B-C, Table 1**).

2.3. The Binding of PI to the Vanilloid Site Normally Increased the Temperature Threshold and Sensitivity of rTRPV1 but Did Not Change the Systemic Thermal Instability

When the resident PI occupies the well-known vanilloid site, rTRPV1 in MSP2N2 cannot open even at 48 °C. This closed state of PI-bound rTRPV1 is almost identical between 4 °C and 48 °C. [14] However, once the PI lipid linked R409, D509, R557, E570 and Q700 together via H-

bonds, there were several differences between PI-bound rTRPV1 at 48 °C and PI-free rTRPV1 at 25 °C (**Figs. 3A-B**).

In the pore domain and its interfaces with the S4-S5 linker and the TRP domain, the E648-K656 and K688-E692 salt bridges were disrupted with the formation of the D576-R579 and Y627-E636-K639 and E692-R575 H-bonds, the K571-E570/E692 salt bridges and the D654-F655 π interaction. In the VSLD, the R491-E513 salt bridge, the R455-Y537-K535 H-bonds, and the F434-F438 and V486-F490 and F489-I493 and Y495-F496/R499 and Y511-L515 π interactions were disrupted. In the meanwhile, the Y441-Y444 and Y463-Y530 and F489-F490 and Y495-E513 π interactions were formed with the Y487-R491 π interaction changing to an H-bond (**Fig. 3A**).

In the VSLD/TRP interface, when the H-bond shifted from R557-T704 to Y554-T704, and the R491-D707 H-bond was disconnected. In the S4-S5 linker/TRP interface, the Q560-K694 H-bond was also broken but the W697-R701 CH-π interaction appeared. In the pre-S1/TRP interfaces, the new E397-K710, Y401-D707, D411-N695 and Q423-R701 H-bonds and the new H410-I696 π interaction were added. Finally, in the pre-S1/VSLD interface, the Q423-D427 and D424-R428 H-bonds were disrupted but a R409-D509 salt bridge was created (**Fig. 3A**). In this case, the total non-covalent interactions and grid sizes along the gating pathway were 67 and 86, respectively. Thus, the systemic thermal instability (T_i) of PI-bound rTRPV1 in MSP2N2 decreased from 1.38 to 1.28 (**Table 1**). If the same open state was employed as a control, the mean structural thermo-sensitivity Ω_{10} would be about 28.8, which was comparable to the Q_{10} value 28.2 (**Table 1**). [14] However, the tight interaction of rTRPV1 with MSP2N2 allowed the PI pocket to be the biggest $Grid_8$ with an 8-atom size (**Fig. 3B**). When two equivalent H-bonds sealed this grid, the calculated melting temperature was about 58 °C (**Table 1**). That may be why the PI-bound rTRPV1 in MSP2N2 cannot open at 48 °C. [14]

Once the E397-K710 and Y401-D707 H-bonds had been broken in a normal lipid environment, the biggest $Grid_{13}$ with a 13-residue size via the shortest path from Y401 to R409, D509, E513, Y495 and R499 and back to Y401 would provide a melting temperature 43 °C as a normal threshold to disrupt the Y401-R499 π interaction and the related R409-D509 salt bridge so as to release the nearby PI lipid from the vanilloid site for rTRPV1 opening (**Table 1, Figs. 3A-D**). In that case, the total non-covalent interactions and grid sizes along the same gating pathway would be 65 and 88, respectively, so that the systemic thermal instability (T_i) of PI-bound rTRPV1

in the native lipid environment would be 1.35, which was similar to that in PI-free rTRPV1 at 25 °C (**Table 1**). If the same open state had been employed as a control, the mean structural thermo-sensitivity Ω_{10} would be about 28.7, which was also comparable to the Q_{10} value 28.2 (**Table 1**). [14] In that regard, the E397-K710 and Y401-D707 H-bonds may inactivate rTRPV1 from a closed state in the presence of MSP2N2.

2.4. PI-free rTRPV1 at 48 °C after 30 s Had a Putatively inactivate State with the Biggest $Grid_{9'}$ in the Pore Domain for a T_m 56 °C

In addition to an open state at 48 °C, a new state at 48 °C after 30 s for PI-free rTRPV1 (EMD 23478, PDB-7LPD) has been proposed as a pre-open closed state when its major class for 10 s (EMD-23477) was similar to its minor class for 30 s [14] If the open state was used a control, the same broken Y401-R499 π interaction in $Grid_{21}$ resulted in different changes along the gating pathway of this minor class (PDB-7LPD). For example, the Y401-E397 π interaction was present in the pre-S1 domain. On the other hand in the VSLD, the R499-D509 salt bridge and the Y495-S510 H-bond were observed but the F434-F438 and F489-F490 and Y495-F496 and F517-F496/L521 π interactions were disrupted. Meanwhile, the F438-Y555 and Y441-F488 and P456-Y463 and F489-I493 and Y530-F531 and Y554-Y555 π interactions and the Y463-K535/Y537 H-bonds and the R534-E536 salt bridge were restored with the new Y441-Q519 and R491-Q494 H-bonds and the Y495-E513 and Y463-Y530 π interactions. As a result, the F559-F438 π interaction in the S4-S5 linker/VSLD interface was broken, the H-bond moved from R557-E570 to E570-Q700 in the VSLD/S4-S5 linker/TRP interfaces, and the W697-R701 CH-π interaction became a strong cation-π interaction. Finally, when the conformational change extended to the outer pore, the E636-K639 salt bridge changed to an H-bond and the H-bonding pair moved from T650-N652 to E651-Y653. Of special note, the formation of the H410-E692 π interaction and the N695-H410 and Y401-D707 H-bond and the E397-K710 salt bridge in the pre-S1/TRP interface was reminiscent of the similar or same non-covalent interactions in PI-bound rTRPV1 in the presence of MSP2N2 at 48 °C (**Figs. 3A, 4A**).

Taken together, when the biggest $Grid_{9'}$ in the pore domain with a 9-residue size controlled the D576-T685 H-bond and the F580-L678 π interaction at the S5/S6 interface via the shortest path from D576 to F580, L678, T685 and back to D576 (**Figs. 4A-C, E**), the resultant melting temperature T_m was about 56 °C, the same as that of the open state (**Table 1**). On the other hand, when the total non-covalent interactions and grid sizes along the gating pathway from D388 to

K710 significantly changed from 46 and 66 to 60 and 59, respectively (**Fig. 2A, 4A**), the calculated Ω_{10} had a range from -2.07 to -21.3 and a mean value -5.10 (**Table 1**), which was close to the experimental Q_{10} of the inactivated state (-5.09). [18] Further, this new state had the lower systemic thermal instability (T_i = 0.98) than those of the closed state at 25 °C and the open state at 48 °C (Ti=1.38, 1.43, respectively) (**Table 1**). Finally, the putative inactivating Y401-D707 and E397-K710 bridges as found in PI-bound rTRPV1 at 48 °C were also present in this new state (**Figs. 1A, 3A, 4D-E**). Accordingly, the major class for 10 s may be a pre-open closed state but the similar minor class for 30 s may serve as a putative inactivated state from the pre-open closed state and would become a major class after 50 s (**Fig. 5A**). [19]

3. DISCUSSION

TRPV1 is designed and created as a bio-thermometer in the thermostable system to detect noxious heat and to protect human or animal bodies from heat damage. [1-4] To this end, it should meet several protein engineering requirements. First, it should be an integral membrane protein with a relative high physicochemical stability or heat capacity to avoid thermal denaturation. Second, it should be an ion channel that can directly couple a temperature signal to an electronical signal reporter for a readout by a primary afferent sensory neuron. Third, its opening from the closed state within 10 °C apart should have a high Q_{10} with a steep response to a small change in a surrounding predetermined temperature. Fourth, it should have a heat switch with two temperature threshold limits for two gating states, one for activation to sense noxious heat and the other for inactivation to alleviate pain by exploiting the use-dependent desensitization upon constant or repeated noxious heat stimuli. In the biochemical and biophysical world, a topological DNA hairpin-like grid in a grid-like non-covalently interacting mesh network may be an ideal tool for thermosensitive TRP channels to achieve them.

The DNA hairpin loop with the limited lengths has been designed as a temperature switch, a thermometer and an ionic detector with Q_{10} in the range from 1.8 to 2.7. [20] Its oligonucleotides with complementary nucleotide sequences at the ends form a duplex region as the hairpin stem upon intra-strand hybridization, and its nucleotides in between as the hairpin loop. When a temperature increases above a threshold, the DNA hairpin melts and thus becomes single stranded. Its melting temperature threshold sharply depends on the H-bonded and stacked base pairs in the stem, the length and flexibility of the loop and the ionic strength in a solution. Generally, a stable stem or a small and rigid loop or a high salt concentration in the solution allows the DNA hairpin

to have a high threshold to sense and to respond to highly specific and small changes in an environmental temperature. When the loop length is decreased from 20 to 10 A's or the H-bonded G-C base-pairs raise from 2 to 4, the melting temperature threshold can be increased more than 20 degrees. Clearly, a short stem favors sharp hairpin melting rather than gradual melting. Since a change in the loop sequence has no significant effect on the temperature threshold of the DNA biosensor, [20] once non-covalent interactions in a single subunit create a single topological grid in the mesh network of protein with a minimal circle, its grid thermodynamics should be comparable a DNA hairpin.

Like the DNA hairpin thermal biosensor, at a given physiological salt concentration (150 mM NaCl), when non-covalent interactions made the biggest grid along the gating pathway from D388 in the pre-S1 domain to K710 in the TRP domain of rTRPV1, the melting temperature T_m increased with a decreased size and an increased number of equivalent H-bonds to seal the grid. In the absence of the PI lipid at the vanilloid site, rTRPV1 had the biggest $Grid_{21}$ to control the R499-Y401 π interaction via the shortest path from Y401 to Q423, D427, W426, F434, Y555, Y441, F516, F517, F496, R499, and back to Y401 in the pre-S1/VSLD/ interface (**Fig. 1**). As the grid size was 21 residues and two equivalent H-bonds kept this $Grid_{21}$, the melting temperature T_m was about 32 °C (**Table 1**). Therefore, its melting at 48 °C further disrupted the R499-Y401 π interaction in the grid and resulted in the formation of the biggest $Grid_9$ with a 9-residue size via the shortest path from R557 to E570, Q560, W697, R701, Q700 and back to R557 in the open state (**Fig. 2**). When two equivalent H-bonds controlled the R557-E570 H-bond, a melting temperature threshold was at about 56 °C (**Table 1**). Similarly, the biggest $Grid_{9'}$ in the putative inactivated state also had the same 56 °C as T_m when two equivalent H-bonds sealed the 9-residue grid via the shortest path from D576 to F580, L678, T680 and back to D576 (**Fig. 4, Table 1**).

On the other hand, in the absence of the E397-K710 and Y401-D707 H-bonds in a native lipid environment, the biggest $Grid_{13}$ would have a normal melting temperature 43 °C for channel opening when 1.5 equivalent H-bonds sealed a 13-residue grid via the shortest path from Y401 to R409, D509, E513, Y495, R499 and back to Y401 (**Table 1, Fig. 3**). Like $Grid_{21}$, its melting above 43 °C may disrupt the R499-Y401 π interaction in favor of channel opening (**Fig. 5A**). In agreement with this proposal, in the presence of the putative biggest $Grid_{12}$ with a 12-residue size via the shortest path from Y408 to R415, D517, E521, Y503, R507 and back to Y408 (**Fig. 4D**), platypus (*Ornithorhynchus anatinus*) TRPV1 (pTRPV1) decreases an activation threshold by

about 3 °C. [19] When the salt concentration was lowered down from 150 mM to 130 mM, the threshold may also decrease from 42 °C to 37.7 °C. [8, 19] However, once PI-bound rTRPV1 was reconstituted in MSP2N2, the presence of those two H-bonds allowed the PI pocket at the vanilloid site to be the biggest $Grid_8$ with an 8-atom size and 2 equivalent H-bonds in it. The resultant high melting temperature 58 °C in such a lipid system may inhibit the release of PI from the vanilloid site at 48 °C for channel opening unless a vanilloid compound like capsaicin could bind near D509 and R557 to compete off the PI lipid (**Table 1, Fig. 3**). [14, 16] Further structural and electrophysiological experiments are necessary to examine the roles of the Y401-R499 π interaction and the R409-D509 salt bridge in securing the normal temperature threshold 42 °C for rTRPV1 opening.

Despite four active biggest grids in rTRPV1 below 58 °C, their roles in gating states may be different. Like a DNA hairpin, a single-step melting reaction of the biggest grid may be rate-limiting for the specific temperature-dependent threshold (T_{th}) in rTRPV1. In accordance with this proposal, $Grid_{21}$ and $Grid_{13}$ may be closely coupled to the lower S6 gate via the R499-Y401 π interaction in the VSLD/pre-S1 interface. Therefore, their melting disrupted this non-covalent bridge, allowing PI-free and PI-bound rTRPV1 to open above 32 °C and 43 °C, respectively (**Table 1, Figs. 1-2**). In contrast, $Grid_9$ may favor the open state by uplifting the S4-S5 linker against the S6 gate via the stimulatory R557-E570 H-bond in the VSLD/S4-S5 linker interface. As the mutation R557E/A/L or E570L/A can disrupt the stimulatory R557-E570 H-bond, it is reasonable that the R557E or E570L mutant leads to a complete loss of function, or mutants R557A/L and E570A or nearby M572A have low heat sensitivity, or E570A increases the threshold from 41.5 °C to 44.3 °C. [14, 24, 25] Since $Grid_9$ had an upper melting temperature limit 56 °C to keep the open state of rTRPV1 (**Figs. 2, 5A, Table 1**), it is reasonable that rTRPV1 exhibits the maximal activity at about 56 °C in response to a temperature ramp from 20 °C to 60 °C. [18] Unlike $Grid_9$, $Grid_{9'}$ was present in all the states of PI-free rTRPV1 unless the D576-R579 H-bond in the closed PI-bound rTRPV1 reduced the size to 6 residues (**Figs. 1A, 2A, 3A, 4A**). Since the residues in this grid are conserved in TRPV1-6, it may serve as a key common anchor to maintain an active pore domain. [11, 26] In direct line with this notion, the mutant R579E is not functional and the D576N/R or R579A mutant is less sensitive to heat than wild type rTRPV1, [24] and rTRPV1 deactivates above 56 °C. [18] Taking all these into account, rTRPV1 may have a bio-thermometer range from 43 °C to 56 °C to monitor noxious heat (**Fig. 5A**).

In addition to the above biggest grids, several smallest grids with a 0-residue size may also be required for channel gating. The first via the shortest path from Y444 to M445, W549, T449, F448 and back to Y544 was highly conserved in the VSLD of all the gating states and thus may serve as a static anchor (**Figs. 1-5**). The second via the shortest path from Y441 and through F516 and Y554 and Y555 and back to Y441 in the VSLD was shared by both closed and open states (**Figs 1-2, 5B**), and the related aromatic residues were highly conserved in thermosensitive TRPV1-4 but not in non-thermosensitive TRPV5-6. [11, 26] Such tight π interactions may allow both smallest grids to serve as relatively stationary anchors against which the S4–S5 linker can uplift in favor of TRPV1 opening. In support of this notion, the Y441S, Y444S, M445W, Y554A or Y555S mutation leaves the channel not functional. [24, 27] The third linked W426 on pre-S1, F434 and F438 on S1, F559 and Q560 in the S4-S5 linker, and W697 and R701 in the TRP domain together via the shortest path. This $Grid_0$ may play a critical role in stabilizing the open state (**Figs. 2, 5B**). The fourth via the shortest path from Y584 to T641 and F640 and Y666 and back to Y584 was present in the pore domain of the open and putatively desensitized states. (**Fig. 5B**). The residues for this smallest $Grid_0$ were also highly conserved in TRPV1-4 but not in TRPV5-6. [11, 26] In agreement with its importance, the Y666A mutation is not functional while the F640L or T641S mutation decreases the temperature threshold to allow either to be constitutively active at room temperature. [28-29] The fifth may stabilize the open state by linking F649, F659, Y653, K656, E651, N652, T650 together against a highly-conserved anchor $Grid_8$ via the shortest path from Y627 to F649 and E636 and back to Y627 in the pore domain (**Figs. 2A, 5B**). It has been reported that the N628K or N652T or Y653T or combined mutation increases the temperature threshold, and the triple mutant N628K/N652T/Y653T has the longer opening durations. [7] Furthermore, the N628L mutation greatly decreases the heat sensitivity ($Q_{10} \sim 2.6$) but the N628D mutation has the opposite effect ($Q_{10} \sim 86$), [14] possibly by mediating the thermal stability of these two smaller grids through ionic interactions with nearby E636. On the other hand, the turret deletion or replacement with glycine between G603 and N626 in mouse TRPV1 (mTRPV1) decreases the temperature threshold to a different extent, [8] possibly by weakening the corresponding R500-Y402 π interaction in the VSLD/pre-S1 interface or generating another new biggest grid with a size larger than 13 residues along the gating pathway from D389 to K711. Thus, the local thermal sensor may act like a bubble in a liquid and any minimal perturbation in the liquid may shift it. Notably, although the deletion of the turret (Δ604-626) still allows the TRPV1 mutant

construct to be activated by heat, the binding of external double-knot toxin or vanilla-toxin (DkTX) to the outer pore prevents heat activation, [9, 15] possibly by affecting the grids in the outer pore (**Fig. 5**). Altogether, both the biggest and smaller grids may be important for heat-gated TRPV1.

When PI-free rTRPV1 opens at 48 °C from a closed state at 25 °C, the opening of multiple grids may increase entropy but decrease enthalpy as a result of the decrease in the total non-covalent interactions from 60 to 46 along the gating pathway from D388 to K710 (**Figs. 1-2**). Thus, a small decrease in the Gibbs free energy may be enough for intra-molecular gating rearrangements in the grid-like non-covalent interaction mesh networks to activate TRPV1. However, even if multiple short links in grids were included, such a small decrease may be insufficient to produce a high Q_{10} for noxious heat detection. Therefore, a heat-induced decrease in the total chemical potential of all the grids upon the heat-evoked decrease in the total enthalpy included in the non-covalent interactions along the same gating pathway from a closed state to an open state should be considered. In accordance with this proposal, when the total grid sizes dramatically decreased with the total non-covalent interactions, the resultant mean structural thermo-sensitivity (Ω_{10}) for channel opening was comparable to the functional thermo-sensitivity (Q_{10}). For PI-free rTRPV1, the calculated mean Ω_{10} was about 16.2, while the experimental Q_{10} is about 16.4. For PI-bound rTRPV1, the predicted mean Ω_{10} was about 28.7 which was close to the experimental Q_{10} is 28.2. [1, 14] Thus, the presence of the PI lipid at the vanilloid site may be necessary for the high mean Ω_{10} and Q_{10} [14] When the intensity of a non-covalent interaction ranged from the minimal 0.5 kJ/mol to the maximal 3 kJ/mol, the normal Ω_{10} for channel opening could be in a range from 10.9-134 (**Table 1**). Therefore, any measured Q_{10} values for native rTRPV1 or mTRPV1 may be reasonable in this range. [1, 8, 14, 17-19] It should be noteworthy that even if heat-evoked TRPV1 opening is enthalpy-drive, an increase in the heat capacity (love) as a result of the decrease in the total grid sizes from a closed state to an open state along the same gating pathway may be necessary to secure a minimal decrease in the Gibbs free energy for channel opening with a maximal Q_{10} value. [30]

In contrast, the similar experimental T_{th} (>41 °C) for rTRPV1 activation and inactivation, [18-19] together with the similar structure between the pre-open closed state and the putative inactivated state, [14] and the same calculated melting temperature 56 °C of the biggest grids in both the putative inactivated state and the open state (**Table 1**), suggests that like the inactivation from a pre-open state of the Kv4 channel complexes, [31] both the open state and the putative

inactivated state may originate from the same pre-open closed state upon the release of PI from the vanilloid site (**Fig. 5A**). However, similar Ω_{10} (-5.10) and Q_{10} (-5.09) for inactivation was weaker than similar Ω_{10} (28.7) and Q_{10} (28.2) for channel opening. (**Table 1**). [18]. Thereby, channel opening may be faster than and the putative inactivation (**Fig. 5A**). That may account for why the major class appears at 48 °C for 10 s but the similar minor class was present at 48 °C for 30 s and would become a major class after 50 s. [14, 19] On the other hand, among different gating states, the normal systemic thermal instability (T_i) along the same gating pathway from D388 in the pre-S1 domain to K710 in the TRP domain was about 1.35 to 1.38 in the closed state no matter whether the PI was bound at the vanilloid site (**Table 1**). However, this value was significantly increased up to 1.43 in the open state but decreased to 0.98 in the putative inactivated state (Table 1). Therefore, the pre-open closed state may have a Ti value between 1.35 and 1.43 in favor of fast activation but slow inactivation in an irreversible manner (**Fig. 5A**). [1, 8, 18-19]

Of special note, the smaller $Grid_2$ via the shortest path from Y401 to E397, K710, D707 and back to Y401 may play a pivotal role in inactivating rTRPV1 from the pre-open closed state (Figs. 4A, D, E). In this $Grid_2$, the presence of the Y401-D707 H-bond in the pre-S1/TRP interface may inactivate the channel, alleviating pain upon constant or repeated noxious heat stimuli-induced desensitization (**Table 1, Figs. 2-3**). [1, 8, 14, 18-19] In agreement with this proposal, the thermosensitive dynamic interaction between the N- and C-terminal domains (segments 1-433 and 688-839, respectively) of mTRPV1 but not pTRPV1 triggers a conformational rearrangement in the pore causing desensitization. [19] In contrast, the absence of a serine residue between S410 and E411 may not allow pTRPV1 to have the Y408-D715 H-bond in the pre-S1/TRP interface to inactivate pTRPV1 (**Figs. 3D, 4D-E**). [13, 19, 32] In this regard, the deletion of S404 or the D707A mutation may stop the putative inactivation of rTRPV1, and the cryo-EM structure of pTRPV1 may have unique closed and open states but not an inactivated state around 40 °C in the presence of 150 mM NaCl.

CLOSING REMARK

The topological grids of a grid-like non-covalent interaction mesh network in an ion channel can be used to design a thermosensitive bio-thermometer with a high Q_{10} value. In addition to the ionic strength in the physiological range, the size of the biggest grid and the number and the intensity of the grid size-controlled non-covalent interactions between amino acid side chains in this grid can be used to tune the grid strength for different melting temperature thresholds

to detect distinct minor environmental temperature changes. These non-covalent interactions include salt bridges, aromatic side chain π interactions and H-bonds. Both the biggest and smaller grids along the gating pathway are necessary to control channel gating and the related thermal efficacy. Their opening and closure should be reversible and fast enough to have a very large temperature-dependent effect on channel gating, which can be easily coupled to an electrical readout from the primary afferent sensor neuron. What is more, the use-dependent desensitization may use gating state-dependent systemic thermal instability as a protective measure against noxious heat damage. In this regard, this computational study may render a broad structural basis for thermosensitive TRP channels to work as a bio-thermometer. On the other hand, although a given non-covalent interaction's spatial and geometric requirements have been well-understood, it is still hardly predictable in a complex grid-like temperature-dependent biochemical reaction mesh network. In that regard, this grid thermodynamic model, once examined by the temperature-dependent structural data of TRPV1, may provide more creative metrics for identifying causal structure–activity/selectivity relationships in a supramolecular architecture at a variety of ambient temperatures.

4. METHODS

In this computational study, the topological grids in a grid-like non-covalently interacting mesh network of rTRPV1 below and above the temperature thresholds were analyzed with graph theory as the bio-thermometer basis for noxious heat detection. The *in silico* protomer models were based on the cryo-EM structural data of closed rTRPV1 in MSP2N2 with PI-bound at 4 °C (PDB ID, 7LP9, model resolution = 2.63 Å) and 48 °C (PDB ID, 7LPC, model resolution = 3.07 Å), capsaicin-bound at 25 °C (PDB ID, 7LPB, model resolution = 3.54 Å) and 48 °C for 10 s (EMD-23477, model resolution = 3.70 Å) and 30 s (EMD-23478 or PDB ID, 7LPD, model resolution = 3.55 Å), and open rTRPV1 with capsaicin-bound at 48 °C (PDB ID, 7LPE, model resolution = 3.72 Å), [14] UCSF Chimera was used to assess non-covalent interactions in TRPV1. All the stereo- or regio-selective inter-domain diagonal and intra-domain lateral non-covalent interactions such as salt-bridges and lone pair/CH/cation-π interactions and H-bonds between amino acid side chains along the gating pathway from D388 in the pre-S1 domain to K710 in the TRP domain of rTRPV1 were included to test their potential roles in forming grids to control the specific temperature thresholds for different gating states and to stablize the heat efficacy for the PI lipid-dependent temperature coefficient Q_{10}.

The standard definition of non-covalent interactions was employed as a filter to secure that results could be reproduced with a high sensitivity. A hydrogen bond was considered present when the angle donor-hydrogen-acceptor was within the cut-off of 60°, and when the hydrogen-acceptor distance was within 2.5 Å and the maximal distance was 3.9 Å between a donor and an acceptor. A salt bridge was considered to be formed if the distance between any of the oxygen atoms of acidic residues and the nitrogen atoms of basic residues were within the cut-off distance of 3.2-4 Å in at least one pair. When the geometry was acceptable, a salt bridge was also counted as a hydrogen bonding pair. The face-to-face π-π stacking of two aromatic rings was considered effective once the separation between the π-π planes was ~3.35-4.4 Å, which is close to at least twice the estimated van der Waals radius of carbon (1.7 Å). The edge-to-face π-π interaction of two aromatic rings was considered attractive when the cut-off distance between two aromatic centers was within 4-6.5 Å. Significant cation-π interactions occurred within a distance of 6.0 Å between a cation and an aromatic center. The short effective CH/π distances was 2.65-3.01 Å between aromatic groups, and 2.75-2.89 Å between CH_3 and an aromatic ring. The lone pair-π interaction distance between a lone electron pair and an aromatic ring was within 3-3.7 Å. [33]

After non-covalent interactions were scanned along the gating pathway of rTRPV1 from D388 in the pre-S1 domain to K710 in the TRP domain, graph theory was used as a novel tool to define grids as the smallest topological circles that had the minimal sizes to control non-covalent interactions in grids. All the temperature-dependent grids were geometrically mapped along the gating pathway in the well-established closed and open states and in the putative desensitized state. The primary amino acid sequence line from D388 to K710 was marked in black. An amino acid side chain or an atom of a bound lipid involving a non-covalent interaction along the gating pathway of rTRPV1 was represented as a vertex (v) or a node and marked with an arrow in different colors. The same kind of non-covalent interactions was marked in the same color. Any link between two vertices was represented as an edge in a grid-like biochemical reaction mesh network. A topological grid was formed between two vertices i and j (v_i and v_j), if and only if there was a path from v_i to v_j and a return path from v_j to v_i. The grid size (S) was definded as the minimal number of the total side chains of residues in protein or atoms in the bound lipid that did not take part in any non-covalent interctions in a grid. For a given grid-like biochemical reaction mesh network, the grid size between v_i and v_j was the sum of the shortest return path distance from node j to i because the direct shortest path distance from node i to j was zero when a non-covalent

interaction existed between them. The simplest way to find the grid size was to identify the shortest return path between two vertices *i* and *j* (v_i and v_j) by using the Floyd-Warshall algorithm. [34] For example, in the grid-like biochemical reaction mesh network of Fig.1A, a direct path length from E636 and F649 was zero because there was a CH-π interaction between them. However, there was another shortest return path from F649 to Y627 and back to E636 via a π–π interaction. Therefore, the grid size was 8. After each non-covalent interaction was tracked by a grid size and the uncommon sizes were marked in black, a grid with an x-residue or atom size was denoted as $Grid_x$, and the total non-covalent interactions and grid sizes along the gating pathway of one subunit were shown in black and blue circles beside the mesh network map, respectively.

The temperature threshold (T_{th}) was calculated from a melting temperature T_m of the biggest grid along the gating pathway using the following equation: [20]

$$T_m\ (°C) = 34 + (n - 2) \times 10 + (20 - S_{max}) \times 2 \quad (1)$$

where, n is the total number of the grid size-controlled non-covalent interactions equivalent to H-bonds in the biggest grid, and S_{max} is the size of the biggest grid.

In either gating state, systemic thermal instability (T_i) along the gating pathway was defined using the following equation:

$$T_i = S/N \quad (2)$$

where, S is the total grid sizes along the gating pathway of one subunit in a given gating state; N is the total non-covalent interactions along the same gating pathway of one subunit in the same gating state.

For enthalpy-driven TRPV1 opening, if a thermosensitive TRPV1 channel changes from a fully closed state to a fully open state within a temperature range ΔT, and if the chemical potential of a grid is defined as the maximal potential for equivalent residues in the grid to form a tight β-hairpin with the smallest loop via non-covalent interactions, [35] the grid-based structural thermo-sensitivity ($\Omega_{\Delta T}$) of a single ion channel can be defined and calculated using the following equations:

$$\Omega_{\Delta T} = [(S_c - S_o)E/2]^{(Hc/Ho)} = [(S_c - S_o)E/2]^{[(ENc)/(ENo)]} = [(S_c - S_o)E/2]^{(Nc/No)} \quad (3)$$

where, H_c and H_o are the total enthalpy included in non-covalent interactions in the closed and open states along the same gating pathway of one subunit, respectively; N_c and N_o are the total non-covalent interactions along the same gating pathway of one subunit in the closed and open states, respectively; S_c and S_o are the total grid sizes along the same gating pathway of one subunit

in the closed and open states, respectively. E is the energy intensity of a non-covalent interaction in a range of 0.5-3 kJ/mol. Usually, E is 1 kJ/mol. [33] Thus, $\Omega_{\Delta T}$ reflects a heat-evoked change in the total chemical potential of grids upon a heat-evoked change in the total enthalpy included in non-covalent interactions from a closed state to an open state along the same gating pathway of one subunit. In the putative inactivated state, $\Omega_{\Delta T}$ was calculated when the parameters of the closed stated in this equation were replaced with those of the putative inactivated state.

When ΔT=10 °C, Ω_{10} could be comparable to the functional thermo-sensitivity or the temperature coefficient (Q_{10}) of a single ion channel. Q_{10} was calculated using the following equation:

$$Q_{10} = (X_2/X_1)^{10/(T2-T1)} \quad (4)$$

where, X_1 and X_2 are open probability (P_o) values or reaction rates obtained at temperatures T1 and T2 (measured in kelvin), respectively.

Conventions and Abbreviations: cryo-EM, cryo-electron microscopy; DkTx, double-knot toxin or vanillotoxin; k_d, the dissociation rate; Ω_{10}, structural thermosensitivity; Q_{10}, functional thermo-sensitivity; PI, phosphatidylinositol; P_o, open probability; T_i, thermal instability; T_m, melting temperature; T_{th}, temperature threshold; TRP, transient receptor potential; TRPM8, TRP melastatin 8; TRPV1, TRP vanilloid-1; TRPVi (i=1; 2, 3, 4, 5, 6); hTRPV1, human TRPV1; mTRPV1, mouse TRPV1; pTRPV1, platypus TRPV1; rTRPV1, rat TRPV1; VSLD, voltage-sensor-like domain

References

1. Caterina, M.J. et al. The capsaicin receptor: a heat-activated ion channel in the pain pathway. *Nature* **389,** 816-824 (1997).
2. Davis, J. B. et al. Vanilloid receptor-1 is essential for inflammatory thermal hyperalgesia. *Nature* **405,** 183-187 (2000),
3. Gavva, N. R. et al., Pharmacological blockade of the vanilloid receptor TRPV1 elicits marked hyperthermia in humans. *Pain* **136**, 202-210 (2008).
4. Vandewauw, I. et al. A TRP channel trio mediates acute noxious heat sensing. *Nature*, **555,** 662-666 (2018**).**
5. Chung, M. K., Wang, S. Cold suppresses agonist-induced activation of TRPV1. *J Dent Res.* **90,** 1098-1102 (2011**)**.
6. Jordt, S. E., Julius, D. Molecular basis for species-specific sensitivity to "hot" chili peppers. *Cell* **108,** 421-430 (2002).
7. Grandl, J. et. al. A. Temperature-induced opening of TRPV1 ion channel is stabilized by the pore domain. *Nat Neurosci.* **13,** 708-714 (2010).
8. Cui, Y. et al. Selective disruption of high sensitivity heat activation but not capsaicin activation of TRPV1 channels by pore turret mutations. *J. Gen. Physiol.* **139,** 273-283 (2012).
9. Jara-Oseguera, A., Bae, C., Swartz, K. J. An external sodium ion binding site controls allosteric gating in TRPV1 channels. *Elife* **5,** (2016); 10.7554/eLife.13356.
10. Long, S. B., Campbell, E. B., Mackinnon, R. Crystal structure of a mammalian voltage-dependent Shaker family K^+ channel. *Science* **309**, 897-903 (2005).
11. Liao, M., Cao, E., Julius, D., Cheng, Y. Structure of the TRPV1 ion channel determined by electron cryo-microscopy. *Nature* **504,** 107-112 (2013).
12. Cao, E., Liao, M., Cheng, Y., Julius, D. TRPV1 structures in distinct conformations reveal activation mechanisms. *Nature* **504,** 113-118 (2013).
13. Nadezhdin, K. D. et al. Extracellular cap domain is an essential component of the TRPV1 gating mechanism. *Nat Commun.* **12,** 2154 (2021); 10.1038/s41467-021-22507-3.
14. Kwon, D. H. et al., Heat-dependent opening of TRPV1 in the presence of capsaicin. *Nat Struct Mol Biol*. **28,** 554-563 (2021).
15. Gao, Y., Cao, E., Julius, D., Cheng, Y. TRPV1 structures in nanodiscs reveal mechanisms of ligand and lipid action. *Nature* **534,** 347-351. (2016).

16. Wang, G. Lipid-dependent sequential allosteric activation of heat-sensing TRPV1 channels by anchor-stereoselective “hot” vanilloid compounds and analogs. *Biochem. Biophys. Rep*. **28,** 101109. (2021); 10.1016/j.bbrep.2021.101109.
17. Yao, J., Liu, B., Qin, F. Modular thermal sensors in temperature-gated transient receptor potential (TRP) channels. *PNAS* **108,** 11109‑11114 (2011).
18. Sa´nchez-Moreno, A. et al. Irreversible temperature gating in trpv1 sheds light on channel activation *eLife* **7,** e36372 (2018); 10.7554/eLife.36372.
19. Luo, L. et al. Molecular basis for heat desensitization of TRPV1 ion channels. *Nat Commun.* **10,** 2134 (2019); 10.1038/s41467-019-09965-6. Correction in: *Nat Commun*. **11,** 1798 (2020); 10.1038/s41467-020-15691-1.
20. Jonstrup, A. T., Fredsøe, J., Andersen, A. H. DNA hairpins as temperature switches, thermometers and ionic detectors. *Sensors* **13,** 5937-5944 (2013).
21. Sun, X. Zakharian, E. Regulation of the temperature-dependent activation of transient receptor potential vanilloid 1 (TRPV1) by phospholipids in planar lipid bilayers. *J. Biol. Chem.* **290,** 4741–4747 (2015).
22. Yu, A. C. et al. Physical networks from entropy-driven non-covalent interactions. *Nat Commun*. **12,** 746 (2021); 10.1038/s41467-021-21024-7.
23. Brauchi, S,, Orta, G., Salazar, M., Rosenmann, E., Latorre, R. A hot-sensing cold receptor: C-terminal domain determines thermosensation in transient receptor potential channels. *J Neurosci.* **26,** 4835–4840 (2006).
24. Boukalova, S., Marsakova, L., Teisinger, J., Vlachova, V. Conserved residues within the putative S4–S5 region serve distinct functions among thermosensitive vanilloid transient receptor potential (TRPV) channels. *J. Biol. Chem*. **285,** 41455-41462 (2010).
25. Kim, M. et al. Evidence that the TRPV1 S1-S4 membrane domain contributes to thermosensing. *Nat Commun.* **11,** 4169 (2020); 10.1038/s41467-020-18026-2.
26. Nadezhdin, K. D. et al. Structural mechanism of heat-induced opening of a temperature-sensitive TRP channel. *Nat. Struct. Mol. Biol.* **28,** 564–572 (2021).
27. Boukalova, S., Teisinger, J., Vlachova, V. Protons stabilize the closed conformation of gain-of-function mutants of the TRPV1 channel. *Biochim. Biophys. Acta*. **1833,** 520-528 (2013).

28. Susankova, K., Ettrich, R., Vyklicky, L., Teisinger, J., Vlachova, V. Contribution of the putative inner-pore region to the gating of the transient receptor potential vanilloid subtype1 channel (TRPV1). *J. Neurosci.* **27,** 7578-7585 (2007).
29. Myers, B. R., Bohlen, C. J., Julius, D. A. yeast genetic screen reveals a critical role for the pore helix domain in TRP channel gating. *Neuron* **58,** 362-373 (2008).
30. Clapham, D. E., Miller, C. A thermodynamic framework for understanding temperature sensing by transient receptor potential (TRP) channels. *PNAS* **108,** 19492–19497 (2011).
31. Ye, W., Zhao, H, Dai, Y, Wang, Y, Lo, Y., Jan, L. Y., Lee, C-H., Activation and closed-state inactivation mechanisms of the human voltage-gated K_V4 channel complexes. *Molecular Cell* ***82,*** 2427–2442 (2022).
32. Liu, B. & Qin F. Single-residue molecular switch for high-temperature dependence of vanilloid receptor TRPV3. *Proc. Natl.Acad. Sci. USA.* **114,** 1589–1594. (2017)
33. Neel, A. J., Hilton, M. J., Sigman, M. S. Toste, F. D. Exploiting non-covalent π interactions for catalyst design. *Nature* **543,** 637-645 (2017).
34. Floyd, R. W. Algorithm-97 - Shortest path. *Commun Acm*, **5,** 345–345 (1962).
35. Kiehna, S. E., Waters, M. L. Sequence dependence of β-hairpin structure: Comparison of a salt bridge and an aromatic interaction. *Protein Science* **12,** 2657-2667 (2003).

Acknowledgements

The author's own studies cited in this article were supported by NIDDK Grant (DK45880 to D.C.D.) and Cystic Fibrosis Foundation grant (DAWSON0210) and NIDDK grant (2R56DK056796-10) and American Heart Association (AHA) Grant (10SDG4120011 to GW).

Author contributions

G. W. wrote the main manuscript text, prepared table 1 and figures 1-5, and reviewed the whole manuscript.

Data availability statement: All data generated or analysed during this study are included in this published article.

Competing interests

The author declares no conflict of interest.

Figure legends

Figure 1. **The grid-like non-covalently interacting mesh network along the gating pathway of PI-free rTRPV1 in the closed state at 25 °C.**

A, The topological grids in the systemic fluidic grid-like mesh network. The cryo-EM structure of one subunit in closed rTRPV1 with capsaicin bound at 25 °C (PDB ID, 7LPB) was used for the model.[14] The pore domain, the S4-S5 linker, the TRP domain, the VSLD and the pre-S1 domain are indicated in black. Salt bridges, π interactions, and H-bonds between pairing amino acid side chains along the gating pathway from D388 to K710 are marked in purple, green, and orange, respectively. The grid sizes required to control the relevant non-covalent interactions were calculated with graph theory and labeled in black. The total grid sizes and grid size-controlled non-covalent interactions along the gating pathway are shown in the blue and black circles, respectively. **B,** The location of the biggest $Grid_{21}$ in the TRP/pre-S1/VSLD/TRP interfaces. **C,** The structure of the biggest $Grid_{21}$ with a 21-residue size in the pre-S1/VSLD interface to control the the R499-Y401 π interaction. **D,** The sequence of the biggest $Grid_{21}$ to control the R499-Y401 π interaction in the blue box.

Figure 2. **The grid-like non-covalently interacting mesh network along the gating pathway of PI-free rTRPV1 in the open state at 48 °C.**

A, The topological grids in the systemic fluidic grid-like mesh network. The cryo-EM structure of one subunit in open rTRPV1 with capsaicin bound at 48 °C (PDB ID, 7LPE) was used for the model.[14] The pore domain, the S4-S5 linker, the TRP domain, the VSLD and the pre-S1 domain are indicated in black. Salt bridges, π interactions, and H-bonds between pairing amino acid side chains along the gating pathway from D388 to K710 are marked in purple, green, and orange, respectively. The grid sizes required to control the relevant non-covalent interactions were calculated with graph theory and labeled in black. The total grid sizes and grid size-controlled non-covalent interactions along the gating pathway are shown in the blue and black circles, respectively. **B,** The location of the biggest $Grid_9$. **C,** The structure of the biggest $Grid_9$ with a 9-residue size in the VSLD/S4-S5 linker/TRP interfaces to control the stimulatory R557-E570 H-bond. **D,** The sequences of the biggest $Grid_9$ with a 9-residue size to control the R557-E570 H-bond in the blue boxes, respectively.

Figure 3. **The grid-like non-covalently interacting mesh network along the gating pathway of PI-bound rTRPV1 in the closed state at 48 °C.**

A, The topological grids in the systemic fluidic grid-like mesh network. The cryo-EM structure of one subunit in closed rTRPV1 with PI bound at 48 °C (PDB ID, 7LPC) was used for the model.[14] The pore domain, the S4-S5 linker, the TRP domain, the VSLD and the pre-S1 domain are indicated in black. Salt bridges, π interactions, and H-bonds between pairing amino acid side chains along the gating pathway from D388 to K710 are marked in purple, green, and orange, respectively. The grid sizes required to control the relevant non-covalent interactions were calculated with graph theory and labeled in black. The total grid sizes and grid size-controlled non-covalent interactions along the gating pathway are shown in the blue and black circles, respectively. The dashed lines are absent in the native lipid system. The putative grid sizes in the native lipid system are labled in grey. **B,** The structure of the biggest $Grid_8$ with a 8-atom size for the PI pocket. **C,** The structure of the biggest $Grid_{13}$ with a 13-residue size in the VSLD/pre-S1 interface to control the Y401-R499 cation-π interaction near PI. **D,** The sequences of the biggest $Grid_8$, $Grid_{13}$, $Grid_{12}$ with 8-carbon, 13-residue, and 12-residue sizes to control the PI pocket in rTRPV1, the Y401-R499 π interaction in rTRPV1, and the Y408-R507 π interaction in pTRPV1, respectively. The controlled bridges are marked in the blue rectangles.

Figure 4. **The grid-like non-covalently interacting mesh network along the gating pathway of PI-free rTRPV1 in a putative inactivated state at 48 °C.**

A, The topologocal grids in the systemic fluidic grid-like mesh network. The cryo-EM structure of one subunit of rTRPV1 with capsaicin bound at 48 °C for 30 s (EMD 23478; PDB ID, 7LPD) was used as a model for a putative inactivated state.[14] The pore domain, the S4-S5 linker, the TRP domain, the VSLD and the pre-S1 domain are indicated in black. Salt bridges, π interactions, and H-bonds between pairing amino acid side chains along the gating pathway from D388 to K710 are marked in purple, green, and orange, respectively. The grid sizes required to control the relevant non-covalent interactions were calculated with graph theory and labeled in black. The total grid sizes and grid size-controlled non-covalent interactions along the gating pathway are shown in the blue and black circles, respectively. **B,** The location of the biggest $Grid_{9'}$. **C,** The structure of the biggest $Grid_{9'}$ in the S5/S6 interface to control the D576-T680 H-bond and the

F580-L678 π interaction. D, The putative inactivating $Grid_2$ to govern the Y401-D707 H-bond and the E397-K710 salt bridge. E**,** The sequences of the biggest $Grid_{9'}$ and the putative inactivating $Grid_2$ with 9- and 2-residue sizes to control the non-covalent interactions in the blue rectangles, respectively.

Figure 5. The tentative model for TRPV1 opening and desensitization upon the heat-evoked melting of the biggest grids.

A. The homo-tetrameric cryo-EM structures of rTRPV1 in the resting closed, open, putatively-inactivated and pre-open closed states (PDB ID:7LP9, 7LPE, 7LPD and EMD-23477, respectively) were used for the model. [14] For a convenient view, only two opposite subunits are shown except for the tetrameric pre-open closed state. The dashed rectangles are the membrane areas. In the presence of the PI lipid (blue) at the capsaicin site, rTRPV1 has 1.5 equivalent H-bonds (orrange) to seal the biggest $Grid_{13}$ (red) with a 13-residue size (red) in the VSLD/pre-S1 interface so that rTRPV1 is closed below a threshold 43 °C. When the temperature increases above the threshold 43 °C, rTRPV1 swiftly opens from a pre-open closed state within 30 s upon the melting of the rate-limiting biggest $Grid_{13}$ in the VSLD/pre-S1 interface along with the release of the PI lipid from the vanilloid site. [14, 19] In the meantime, the biggest $Grid_9$ (red) with a 9-residue size (red) and two equivalent H-bond (orrange) is formed in the VSLD/S4-S5 linker/TRP/VSLD interfaces in favor of the open state below a T_m 56 °C. On the other hand, the channel may also slowly inactivate from the same pre-open closed state. [14, 19] In this putative inactivated state, $Grid_{9'}$ (red) with a 9-residue size (red) and two equivalent H-bonds (orrange) in the S5/S6 interface becomes the biggest with a T_m 56 °C. Clearly, the mean systermatic thermal instability (T_i) between 1.35 and 1.43 of the pre-open closed state may faciliate the fast opening. However, the lower T_i (0.98) of the putative inactivate state may allow rTRPV1 to bypass the open state and to inactivate slowly from the pre-open closed state in a irreversable manner at prolonged temperature between 43 °C and 56 °C. [18, 19] **B,** The proposed smaller grids for TRPV1 gating. The grid sizes are shown in the red circles.

Figures

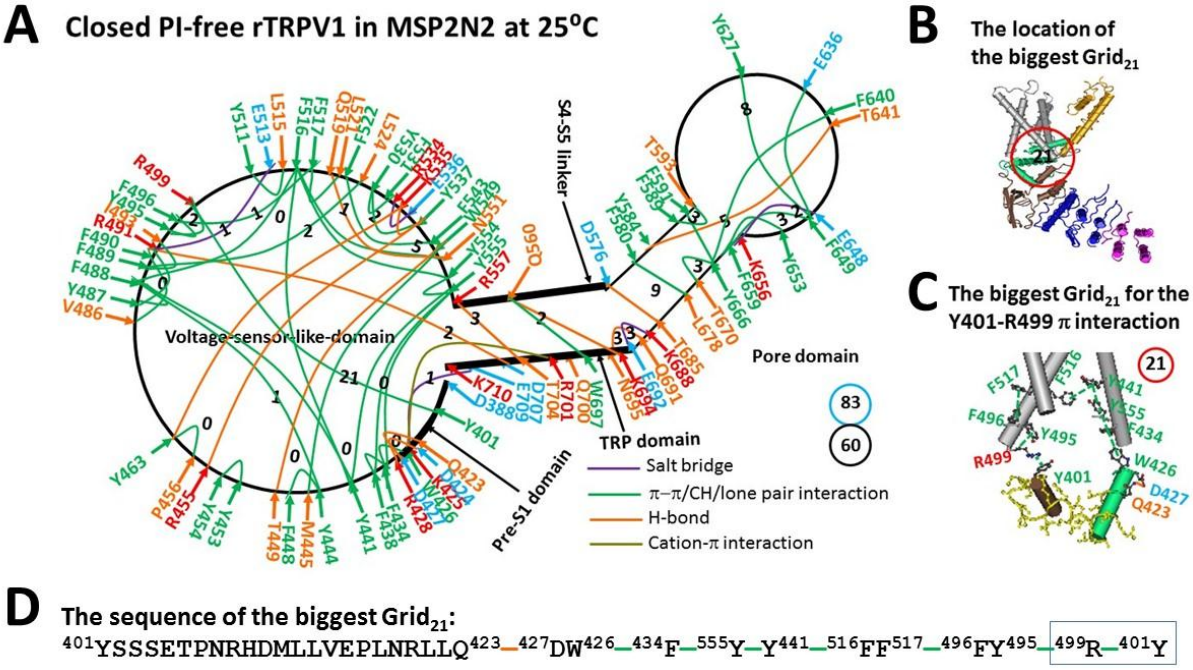

Figure 1

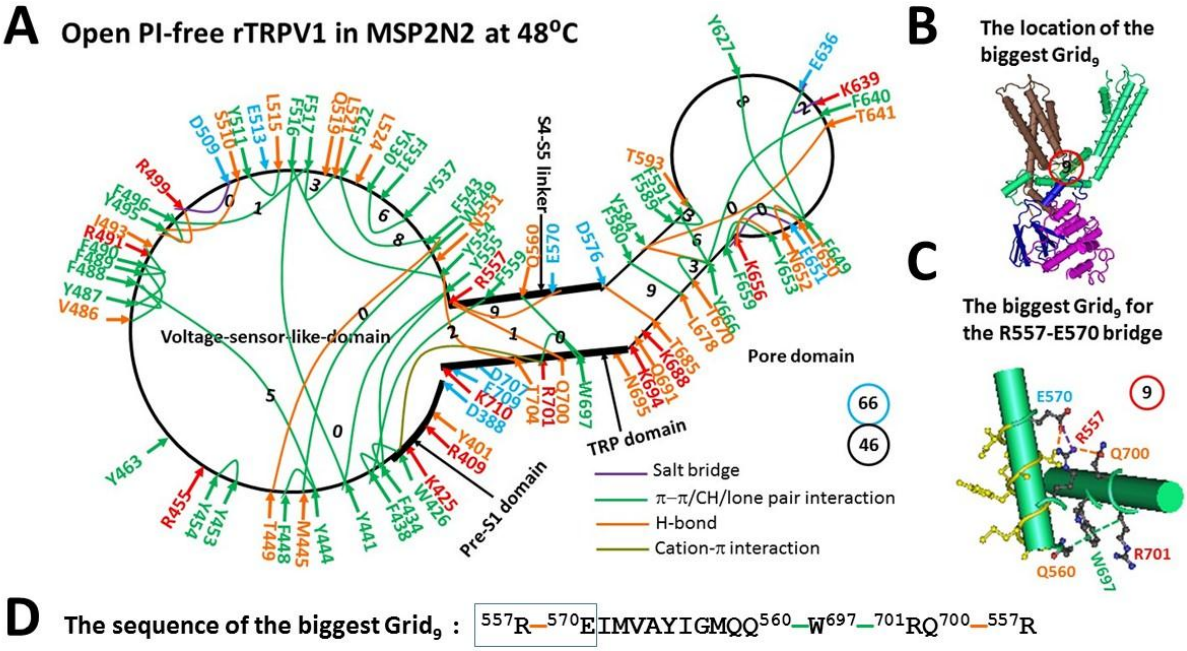

Figure 2

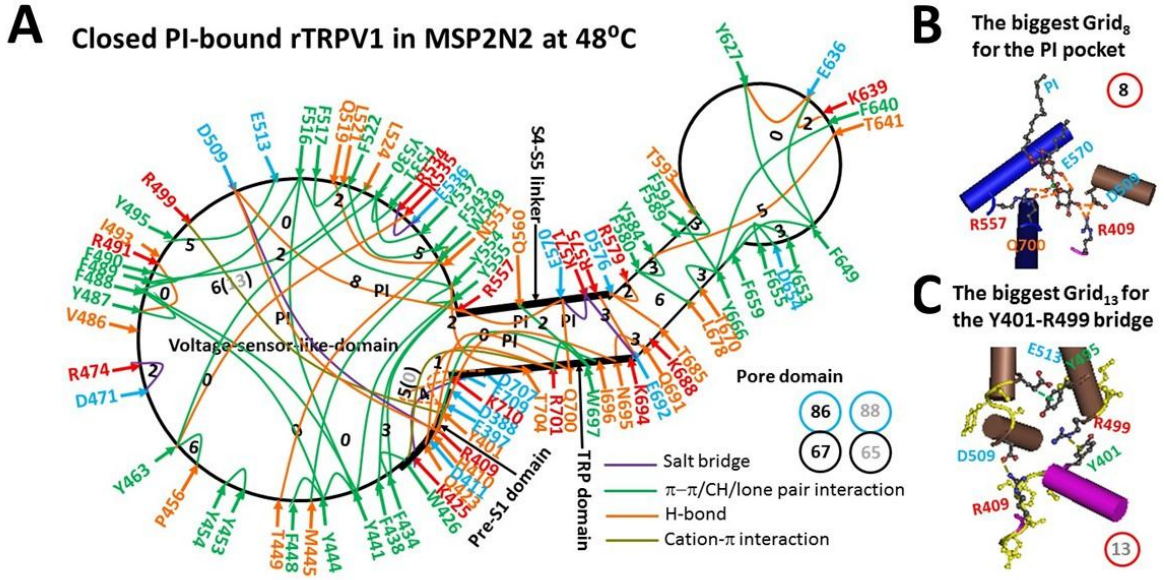

D

rTRPV1 The sequence of the biggest Grid$_8$: PI—^{557}R—PI—^{700}Q—PI—^{409}R—PI—^{509}D—PI—^{570}E—PI

rTRPV1 The sequence of the biggest Grid$_{13}$: ^{401}YSSSETPNR^{409}—^{509}DSYSE^{513}—^{495}YFLQR^{499}—^{401}Y

pTRPV1 The sequence of the biggest Grid$_{12}$: ^{408}YSS ETPNR^{415}—^{517}DSYSE^{521}—^{503}YFLQR^{507}—^{408}Y

Figure 3

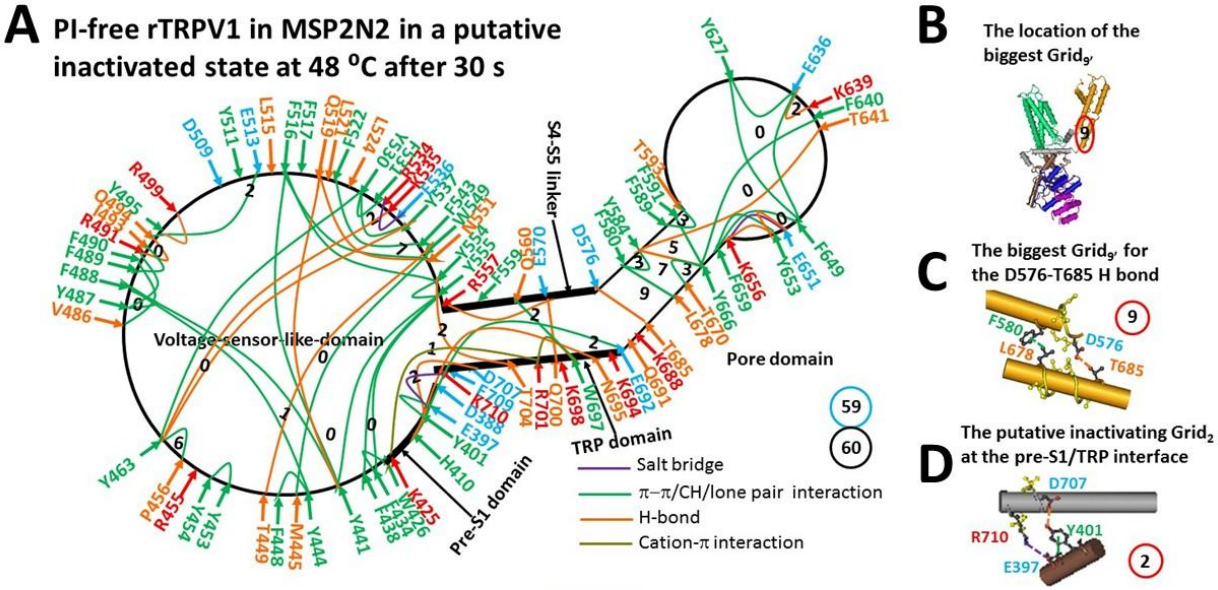

E

The sequence of the biggest Grid$_{9'}$: ^{576}DLCRF^{580}—^{678}LIALMGET^{685}—D^{576}

The sequence of the putative inactivating Grid$_2$: ^{401}Y—^{397}E—^{710}KETD^{707}—^{401}Y

Figure 4

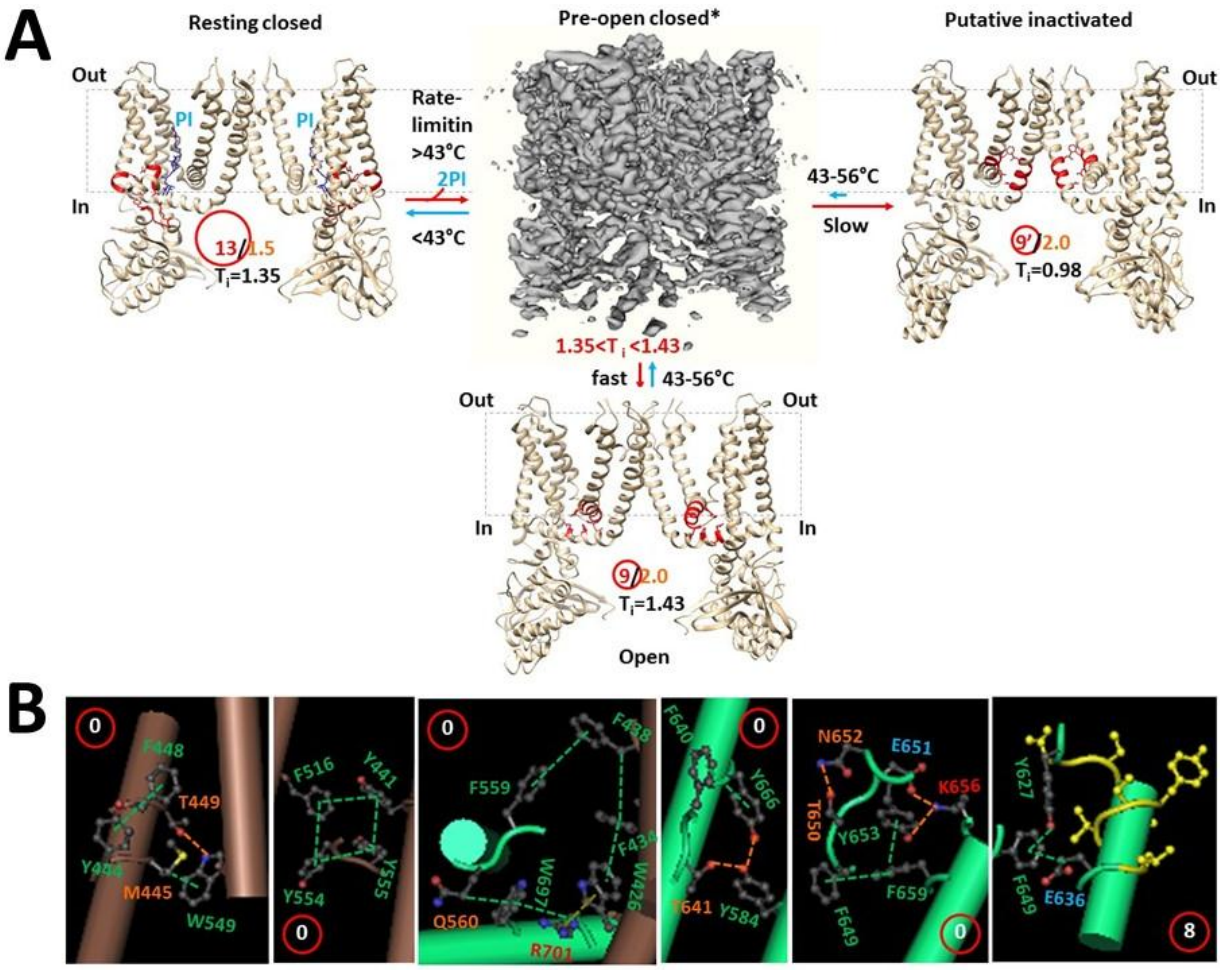
A
Resting closed
Pre-open closed*
Putative inactivated
Out
In
PI
PI
Rate-limitin
>43°C
2PI
<43°C
13/1.5
T_i=1.35
1.35<T_i<1.43
fast
43-56°C
43-56°C
Slow
9'/2.0
T_i=0.98
9/2.0
T_i=1.43
Open
B
F448
T449
Y444
M445
W549
F516
Y441
Y554
Y555
F559
F438
F434
W426
W699
Q560
R701
F640
Y666
T641
Y584
N652
E651
K656
T650
Y653
F659
F649
Y627
E636

Figure 5